Supplementary Information

An evaluation of new particle formation events in Helsinki during a Baltic Sea cyanobacterial summer bloom

Roseline C. Thakur[1], Lubna Dada[1,2,3], Lisa J. Beck[1], Lauriane L.J. Quéléver[1], Tommy Chan[1], Marjan Marbouti[1], Xu-Cheng He[1], Carlton Xavier[1], Juha Sulo[1], Janne Lampilahti[1], Markus Lampimäki[1], Yee Jun Tham[1,11], Nina Sarnela[1], Katrianne Lehtipalo[1,4], Alf Norkko[8,9], Markku Kulmala[1,5,6,7], Mikko Sipilä[1], Tuija Jokinen[1,10]

[1]Institute for Atmospheric and Earth System Research/Physics, Faculty of Science, 00014 University of Helsinki, Helsinki, Finland.

[2]School of Architecture, Civil and Environmental Engineering, École Polytechnique Fédérale de Lausanne, Lausanne, Switzerland

[3]Laboratory of Atmospheric Chemistry, Paul Scherrer Institute, 5232 Villigen PSI, Switzerland

[4]Finnish Meteorological Institute, Helsinki, Finland.

[5]Aerosol and Haze Laboratory, Beijing Advanced Innovation Center for Soft Matter Science and Engineering, Beijing University of Chemical Technology, 100089 Beijing, China.

[6]Joint International Research Laboratory of Atmospheric and Earth System Sciences, Nanjing University, 210023 Nanjing, China.

[7]Lomonosov Moscow State University, Faculty of Geography, 119991, Moscow, GSP-1, 1 Leninskiye Gory.

[8]Tvärminne Zoological Station, University of Helsinki, J.A. Palméns väg 260, FI-10900 Hangö, Finland

[9]Baltic Sea Centre, Stockholm University, Stockholm, Sweden

[10]Climate & Atmosphere Research Centre (CARE-C), The Cyprus Institute, P.O. Box 27456, Nicosia, CY-1645, Cyprus.

[11]School of Marine Sciences, Sun Yat-Sen University, Zhuhai 519082, China

Table S1 Details of Instruments and other supporting data

Parameter measured	**Technique**	**Instrument**	**Resolution and detection limits**	**Site of Measurement**
SO_2	UV-fluorescence technique	Horiba APSA 360	60 s detection limit: 0.2 ppb	a
NO_x	Chemiluminescence technique + thermal (molybdenum) converter	TEI42S	60 s detection limit: 0.2 ppb	a
O_2	IR-absorption photometer	TEI 49	60 s detection limit: 0.5 ppb	a
Air Temperature	Platinum resistance thermometer	Pt-100	60 s	b
Wind direction	2-D ultrasonic anemometer	Thies Clima ver. 2.1x	10 s	b
Wind Speed	Platinum resistance thermometer + thin film polymer sensor	Vaisala DPA500	4 min	b
Relative humidity	Platinum resistance thermometer + thin film polymer sensor	Vaisala DPA500	4 min	b
Global Radiation	Net radiometer	Kipp & Zonen CNR1	60s	b
Tidal Height	wave buoys		c	Helsinki Suomenlina, Gulf of Bothnia, Northern Baltic Sea

[a] SMEAR III station

[b]roof of university of Helsinki (UHEL) Building (kumpula campus)

[c]Wave height is the vertical difference between the wave through and the wave crest. The significant wave height is calculated as the average of one third of the highest waves from the energy spectrum.

The cloudiness parameter

It is defined as is the ratio of measured global radiation (R_d) divided by the theoretical global irradiance (Rg):

$$P = \frac{R_d}{R_g}$$

The theoretical maximum of global radiation (R_g) is calculated by taking into consideration the latitude of the measurement station and the seasonal solar cycle. P < 0.3 defines a complete cloud coverage and P > 0.7 defines clear-sky conditions .This classification is followed by man previous studies (Perez et al., 1990; Sogacheva et al., 2008; Sánchez et al., 2012).

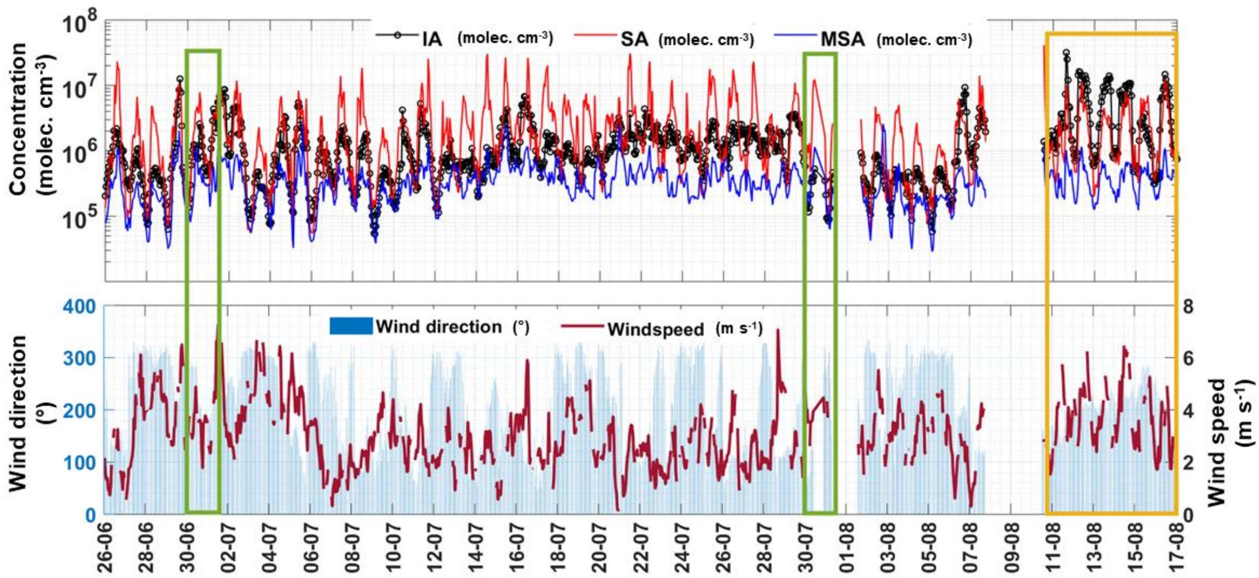

Figure S1: Time series concentration of SA, MSA and IA (60min averaged data) and their variability with changing wind speed and wind direction (30min averaged data). The Green boxes denote the local events and yellow box is covers the time period when the burst/spike events were observed during the study.

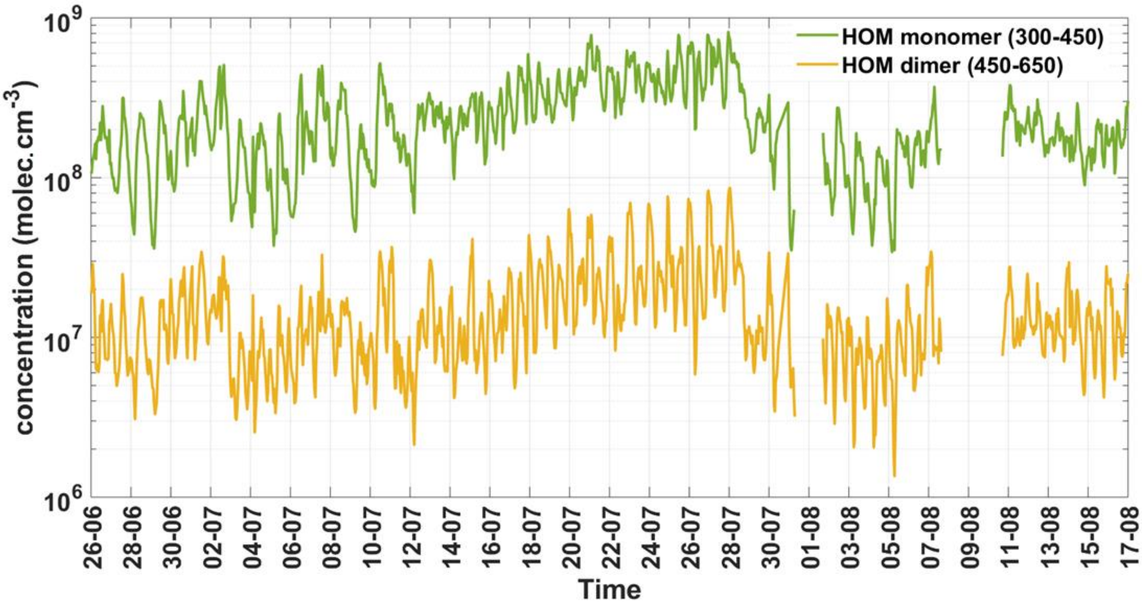

Figure S2: Time series variability in HOM monomer (sum of mass range 300-450 m/z) and dimer (sum of mass range 450-650 m/z) concentration during the study period (60min averaged data from CI-Api-ToF)**.** Note the concentrations are plotted using the unit mass resolution data.

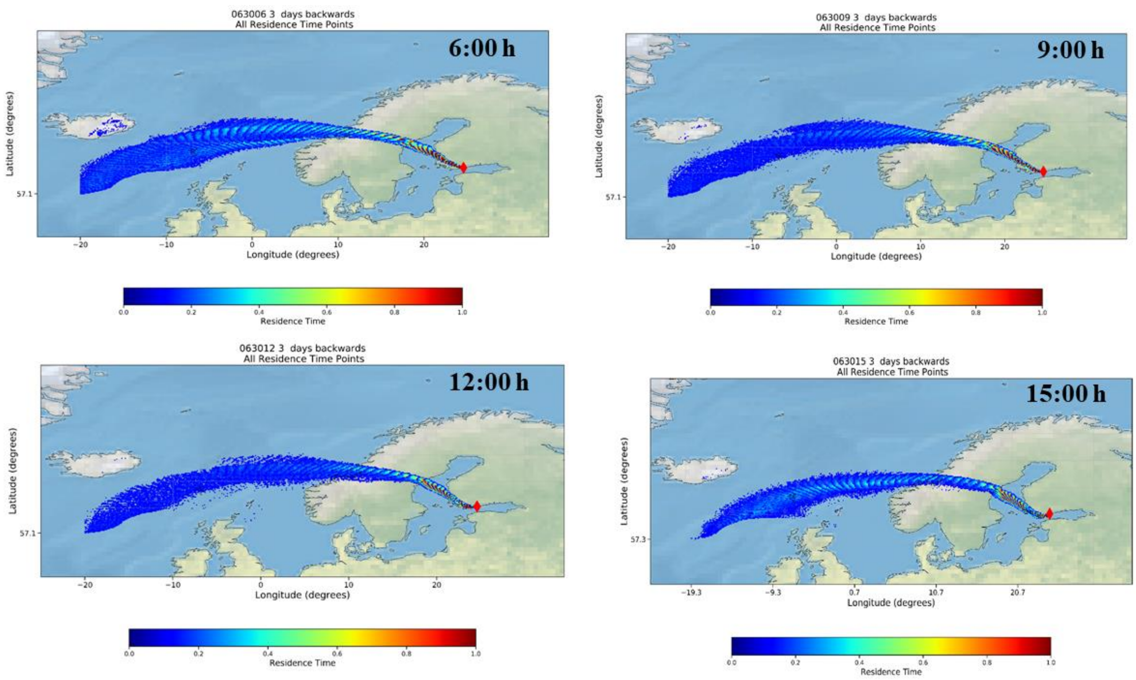

Figure S3: Residence times of air masses (3-day backwards) arriving at the experimental site on 30 June 2019. The color bar indicates the normalized residence times for each subplot. The residence time of particles originating 3 days before reaching SMEAR III is shown for 3:00 h, 6:00 h, 9:00 h and 12:00 h. The red shaded areas indicate the latitude/longitude pairs having the maximum residence time.

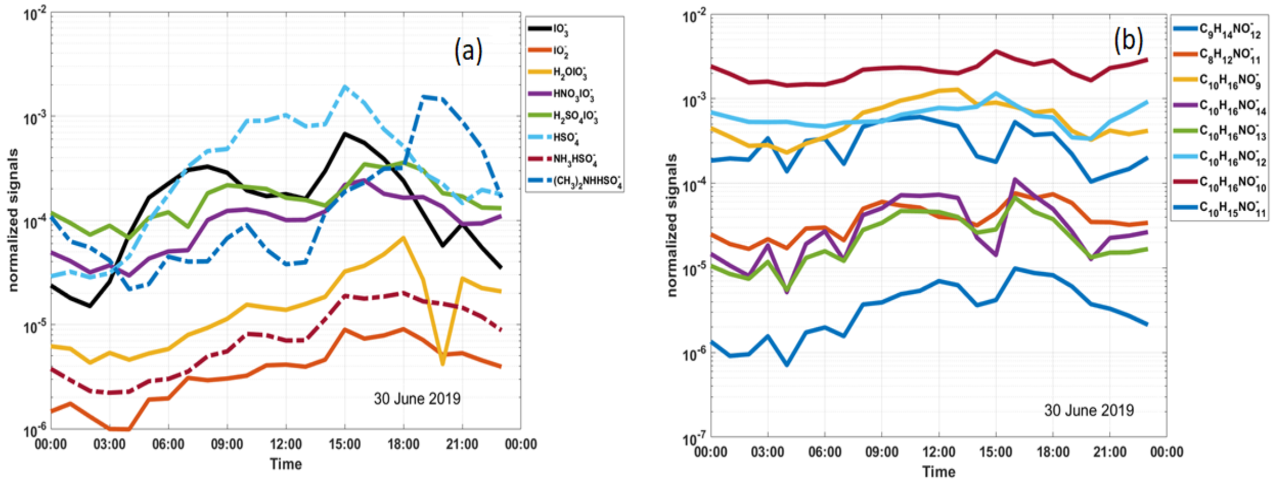

Figure S4: Diurnal variation of the inorganic clusters (a) and organic clusters (b) observed during the NPF event on 30 June 2019 as seen from the spectrum of CI-Api-ToF.

Local/regional event 30 July 2019

Another local/regional event probably driven by SA was observed on 30 July 2019 (Fig. S5a), forming particles, which grew to almost CCN relevant sizes. The growth of ions and particles actually occurred from 07:45 h-11:15 h (Fig. S5a and S5b). By this time, the particles had reached around 50 nm in size (lower limit of CCN).The highest $J_{1.5}$ was 3.7 cm^{-3} s^{-1} was observed at 09:00 h, significantly higher than *J* (ions), indicative of a neutral dominated nucleation event (Fig. S5c). After 11:30 h we observe a group of fragmented burst or spike events without clear growth pattern. No significant variation in formation rates was observed in the positive and the negative mode (Fig. S5b). A clear increase in sub-3 nm (1.25–3.1 nm) particle concentration (from 10^2 to >10^3) is seen during this event and formation rate of the smallest particles ($J_{1.5}$) increases from 0.9 cm^{-3} s^{-1} to 3.8 cm^{-3} s^{-1} between 06:00 -09:00 h indicating cluster formation (neutral nucleation) (Fig. S5c). A 10 times increase in sub 3nm particles is observed once the cluster formation initiated (07:45 h, local time UTC+2 h) when the concentration of SA increases from 8.2×10^6 to 1.2 ×10^7molec. cm^{-3} and The nucleation mode particles how a significacnt increase from ~2000 cm^{-3} to ~10 000 cm^{-3} during the event, however we do not see any significant increase in Aitken and accumulation mode particles. (Fig. S5e). The aitken mode particle concentration starts to increase after a time lag of 40 min. Unfortunately, in this case we cannot discuss on the SA concentration after 12:00 h as data recording was disrupted between 12:30-20:30 h. The highest SA concentration during this event was 1.22 $\times 10^{7}$ molec cm^{-3} as compared to IA and MSA which were one order of magnitude lower than SA (1.15 $\times 10^{6}$ and 5.28 $\times 10^{6}$ molec. cm^{-3}, respectively) (Fig. S5d). The particles reached the size of 40 nm at around 11:30 h after which the event ceases. The condensation sink and the accumulation mode particles remain more or less constantly low, yet we observe a disruption in the event. A change in wind direction from 120° to 200° was observed between 11:30–12:30 h, which lead to the observation that we do not see regional NPF (growing particles) in the changed air mass. The cynobacteria bloom on 30 July 2019 was not much spread in the sea areas (Fig. S5f).

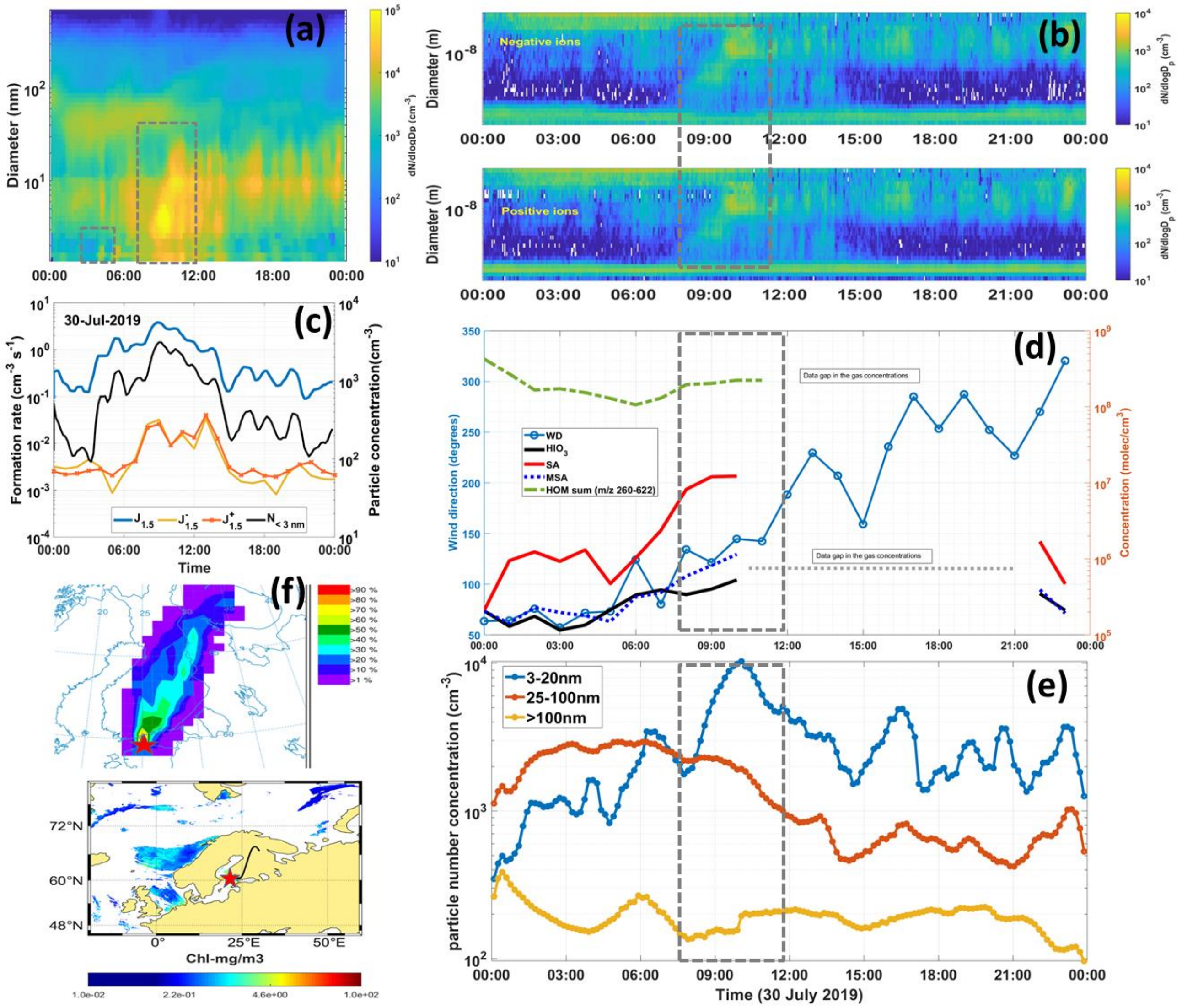

Figure S5: Local/regional Event, 30 July 2019. (a) Number size distribution of particles (data combined from PSM,NAIS and DMPS; size range: sub-3 nm–1000nm). (b) Size distribution of ions during the event (NAIS). (c) formation rates ($J_{1.5}$) of 1.5 nm particles and ions ($J^-_{1.5}$ and $J^+_{1.5}$) particle number concentrations (<3 nm). (d) Dirunal variation of HOMs SA, IA and MSA with wind direction (WD). (e) The concentrationof nucleation (3–10 nm) Aitken (10–100 nm) and accumulation mode (>100nm) particles during the event. (f) Trajectory frequency plot (100 a.g.l, arrival time of trajectory at the measurement site: 22:00 h) for 24 h back trajectory using GDAS meterological input data (frequency grid resolution: $1.0^{\circ} \times 1.0^{\circ}$) and Chl-*a* concentrations (MODIS); Black line shows the trajectory direction and the star point denotes the measurement site. The dashed black lines show denote the time stamp of the nucleation events.

Even in lakes the abundance of cynobacteria was sparse. Only cynobacterial bloom was found in Southern edge of Gulf of Bothania and northern most part of the Baltic sea. The trajectory frequency plots showed that most of the trajectories were from the northern land areas (including urban cities and boreal forests) of Finland (Fig. S5f) with highest residence times over these land regions. Therefore the precursor gases from the cynobacteria bloom, IA and MSA do not show a significant concentration increase during this event and hence are assumed to be contributing insignificantly to this event. The greater residence times over the land areas clearly support SA-driven NPF with possible contribution of organics.

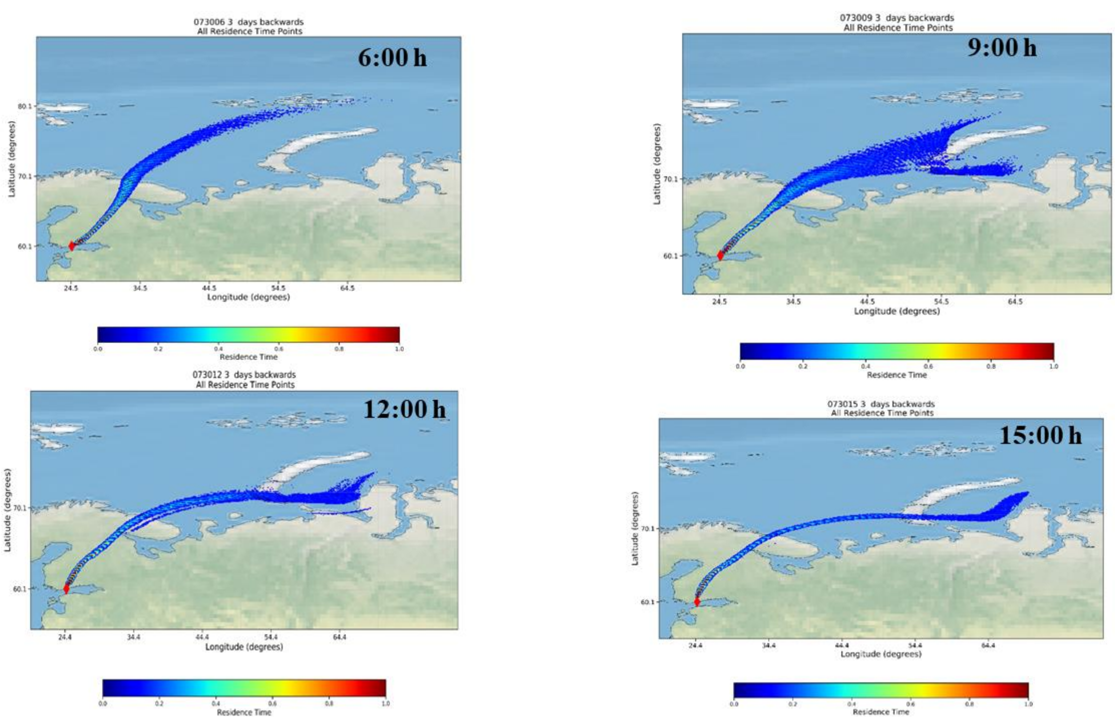

Figure S6: Residence times of Air masses (3-day backwards) arriving at the experimental site on 30 July 2019. The color bar indicates the normalized residence times for each subplot. The residence time of particles originating 3 days before reaching SMEAR III is shown for 6:00 h, 9:00 h, 12:00 h and 15:00 h. The red shaded areas indicate the latitude/longitude pairs having the maximum residence time. Note the highest residence times over the land areas.

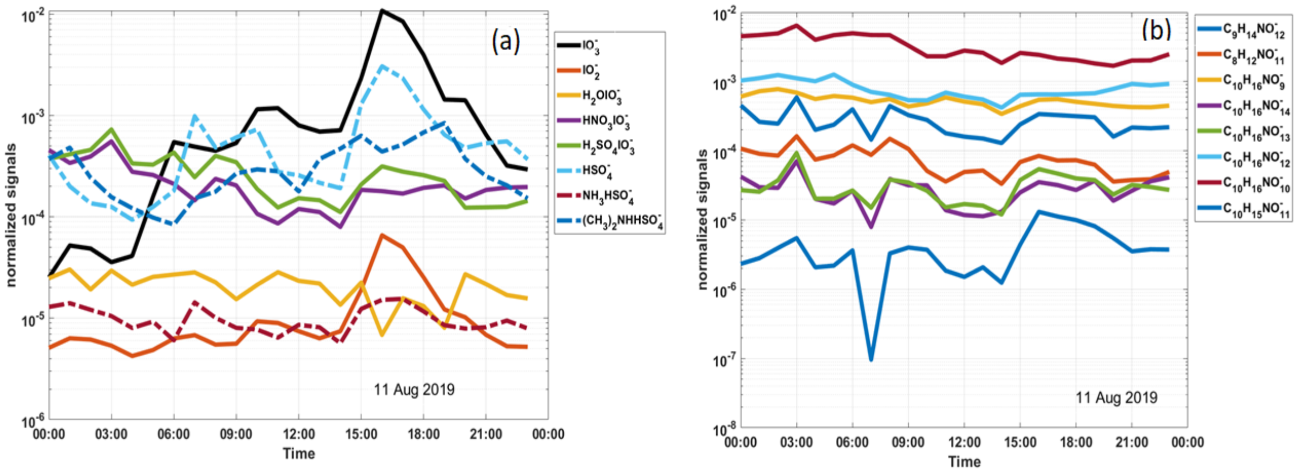

Figure S7: Diurnal variation of the inorganic (a) and organic clusters (b) observed during the NPF event on 11 August 2019.

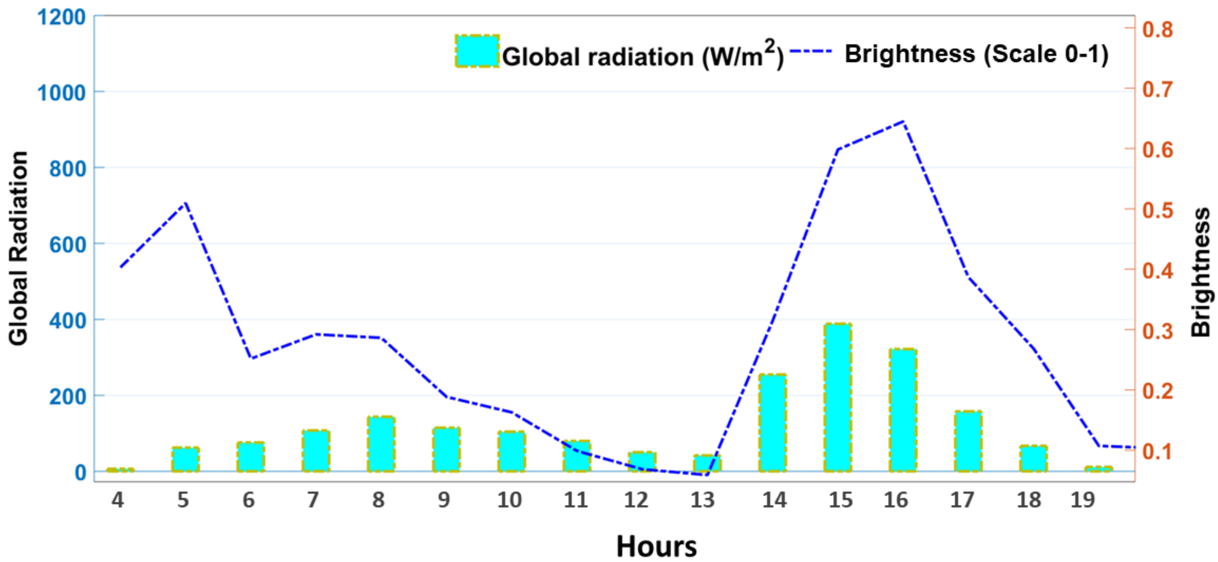

Figure S8: Diurnal variability of global radiation and estimated cloudiness on 11 August 2019. Note the increased radiation and brightness from 14–16 h (time when NPF starts).

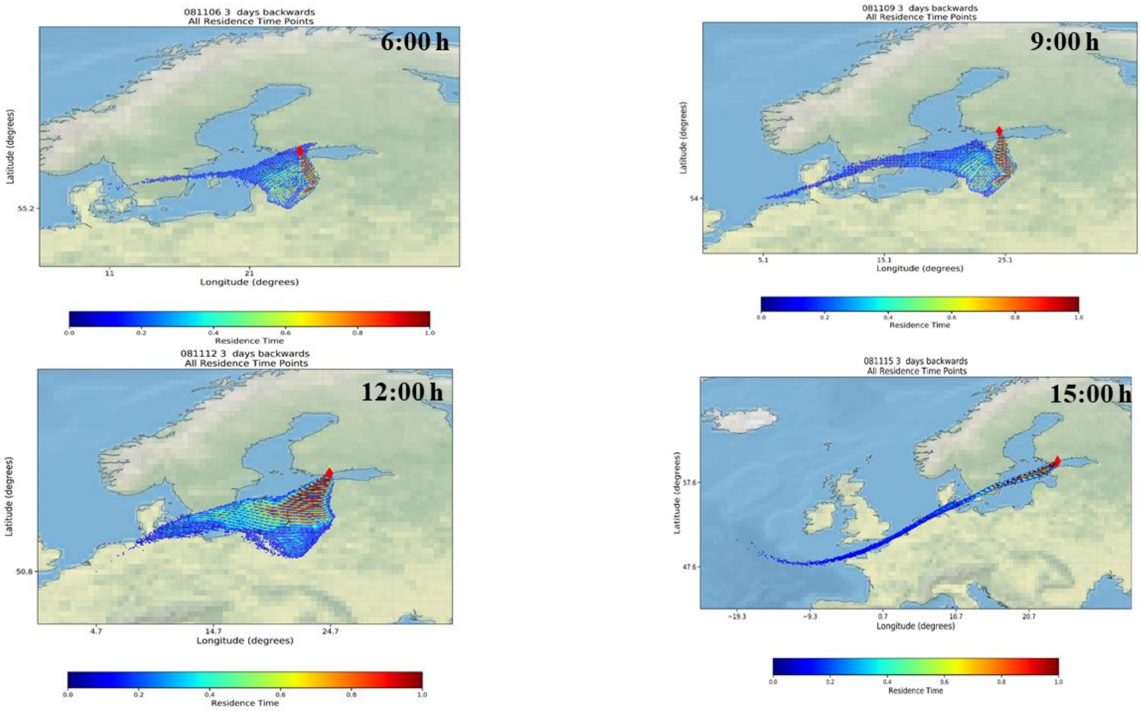

Figure S9: Residence times of air masses (3-day backwards) arriving at the experimental site on 11 August 2019. The color bar indicates the normalized residence times for each subplot. The residence time of particles originating 3 days before reaching SMEAR III is shown for 6:00 h, 9:00 h, 12:00 h and 15:00 h. The red shaded areas indicate the latitude/longitude pairs having the maximum residence time. Note the highest residence times over Baltic Sea region at 15:00 h (highest IA concentration was observed).

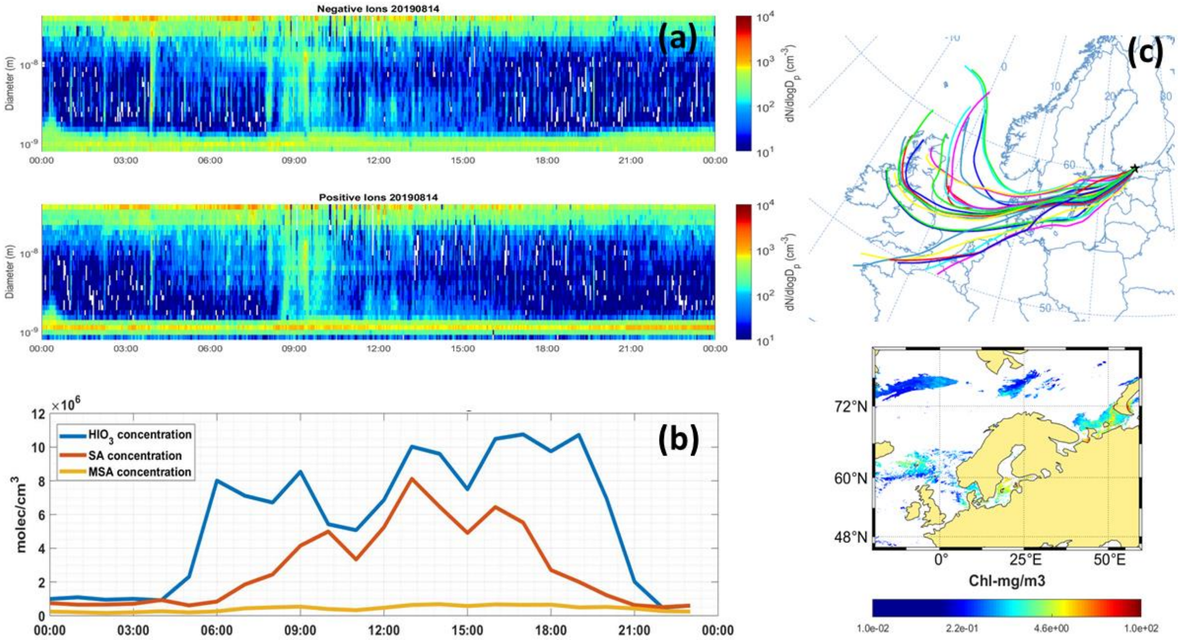

Figure S10: (a) Charged particle number size distribution (negative: upper, positive: lower) obtained from the NAIS. (b) concentration of SA, IA and MSA. (c) Trajectory analyis plot (100 a.g.l) for 24 h back trajectory using GDAS meterological input data (frequency grid resolution: 1.0° × 1.0°) and Chl-*a* concentrations (MODIS) for 14 August 2019.

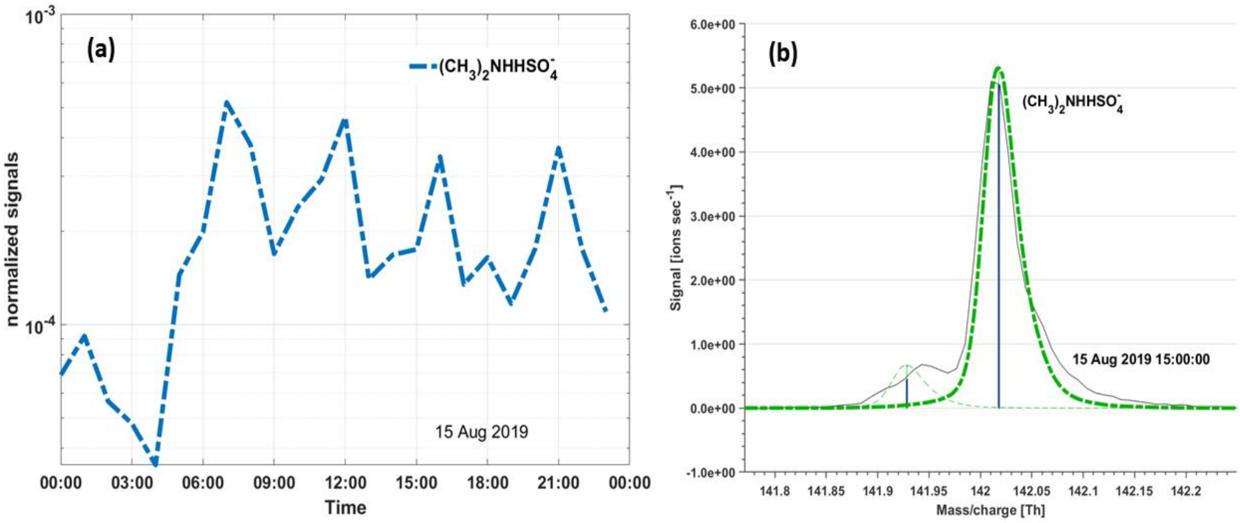

Figure S11: (a) Diurnal variation of the DMA-SA cluster (CI-ApiToF) observed during the NPF event on 15 August 2019. (b) The prominent peak of DMA-SA cluster seen at the peaktime of NPF at 15:00 h.

References:

Perez, R., Ineichen, P., Seals, R., and Zelenka, A.: Making full use of the clearness index for parameterizing hourly insolation conditions, Solar Energ., 45, 111–114, doi:10.1016/0038-092X(90)90036-C, 1990.

Sánchez, G., Serrano, A., and Cancillo, M.: Effect of cloudiness on solar global, solar diffuse and terrestrial downward radiation at Badajoz (Southwestern Spain), Optica pura y aplicada, 45, 33– 38, 2012.

Sogacheva, L., Saukkonen, L., Nilsson, E., Dal Maso, M., Schultz, D. M., De Leeuw, G., and Kulmala, M.: New aerosol particle formation in different synoptic situations at Hyytiälä, southern Finland, Tellus B, 60, 485–494, doi:10.1111/j.1600- 0889.2008.00364.x, 2008.